Journal of
Dental Research

Mechanisms of atomization from rotary dental instruments and its mitigation

Journal:	*Journal of Dental Research*
Manuscript ID	JDR-20-1224.R3
Manuscript Type:	COVID-19 Submission
Date Submitted by the Author:	16-Nov-2020
Complete List of Authors:	Sergis, Antonis; Imperial College London Wade, William; King's College London Gallagher, Jennifer; Kings College London Dental Institute, Population and Patient Health Morrell, Alexander; King's College London Patel, Shanon; Kings College London Dental Institute, Conservative Dentistry Dickinson, Chris; Guy's and St Thomas' Hospitals NHS Trust Nizarali, Najla; Guy's and St Thomas' Hospitals NHS Trust Whaites, Eric; Guy's and St Thomas' Hospitals NHS Trust Johnson, Joanna; Guy's and St Thomas' Hospitals NHS Trust Addison, Owen; King's College London, Centre for Oral, Clinical & Translational Sciences Hardalupas, Yannis; Imperial College London
Keywords:	Infection control, Infectious disease(s), Operative dentistry, Bioengineering, Biophysics
Abstract:	Introduction: Since the onset of COVID-19 the potential risk of dental procedural generated spray emissions (including aerosols and splatters), for SARS-CoV-2 transmission, has challenged care providers and policy makers alike. New studies have described the production and dissemination of sprays during simulated dental procedures but findings lack generalisability beyond their measurements setting. This study aims to describe the fundamental mechanisms associated with spray production from rotary dental instrumentation with particular focus on what are currently considered as high risk components; namely the production of small droplets that may remain suspended in the room environment for extended periods and the dispersal of high velocity droplets resulting in formites at distant surfaces. Methods: Procedural sprays were parametrically studied with variables including rotation speed, burr to tooth contact and coolant pre-misting modified and visualised using high speed imaging and broadband or monochromatic laser light-sheet illumination. Droplet velocities were estimated and probability density maps for all laser illuminated sprays generated. The impact of varying the coolant parameters on heating during instrumentation was considered. Results: Complex structured sprays were produced by water-cooled rotary instruments which in the worst case of an air-turbine, included

	droplet projection speeds in excess of 12 m/s and the formation of millions of small droplets which may remain suspended. Elimination of pre-misting (mixing of coolant water and air prior to burr contact) resulted in significant reduction in small droplets but radial atomization may still occur and is modified by burr to tooth contact. Spatial probability distribution mapping identified a threshold for rotation speeds for radial atomization between 80 and 100,000rpm. In this operatory mode, cutting efficiency is reduced but sufficient coolant effectiveness appears to be maintained. Conclusion: Multiple mechanisms for atomization of fluids from rotatory instrumentation exist but parameters can be controlled to modify key spray characteristics during the current crisis.

Date submitted: 9/9/2020

Date last revised: 11/16/2020

Date accepted: 11/17/2020

Mechanisms of atomization from rotary dental instruments and its mitigation

Antonis Sergis[1], William G. Wade[2], Jennifer E Gallagher[2], Alexander P. Morrell[3], Shanon Patel[3], Chris M Dickinson[4], Najla Nizarali[4], Eric Whaites[4], Joanna Johnson[4], Owen Addison[3,4,#,*], Yannis Hardalupas[1,#]

1. Department of Mechanical Engineering, Imperial College London, United Kingdom

2. Centre for Host-Microbiome Interactions, Faculty of Dental, Oral & Craniofacial Sciences, King's College London, London, United Kingdom

3. Centre for Oral, Clinical & Translational Sciences, Faculty of Dental, Oral & Craniofacial Sciences, King's College London, London, United Kingdom

4. Dental Directorate, Guy's and St Thomas, NHS Foundation Trust, London, United Kingdom

co-last authors

Corresponding author

* Faculty of Dental, Oral & Craniofacial Sciences,
King's College London,
Guy's Tower, Guy's Hospital
London, SE1 9RT
United Kingdom
owen.addison@kcl.ac.uk

Keywords: 'aerosol'; 'SARS-CoV-2'; 'infection control'; 'aerosol generating procedure'; 'dental drill'; 'imaging'

Abstract

Introduction: Since the onset of COVID-19 the potential risk of dental procedural generated spray emissions (including aerosols and splatters), for SARS-CoV-2 transmission, has challenged care providers and policy makers alike. New studies have described the production and dissemination of sprays during simulated dental procedures but findings lack generalisability beyond their measurements setting. This study aims to describe the fundamental mechanisms associated with spray production from rotary dental instrumentation with particular focus on what are currently considered as high risk components; namely the production of small droplets that may remain suspended in the room environment for extended periods and the dispersal of high velocity droplets resulting in formites at distant surfaces.

Methods: Procedural sprays were parametrically studied with variables including rotation speed, burr to tooth contact and coolant pre-misting modified and visualised using high speed imaging and broadband or monochromatic laser light-sheet illumination. Droplet velocities were estimated and probability density maps for all laser illuminated sprays generated. The impact of varying the coolant parameters on heating during instrumentation was considered.

Results: Complex structured sprays were produced by water-cooled rotary instruments which in the worst case of an air-turbine, included droplet projection speeds in excess of 12 m/s and the formation of millions of small droplets which may remain suspended. Elimination of pre-misting (mixing of coolant water and air prior to burr contact) resulted in significant reduction in small droplets but radial atomization may still occur and is modified by burr to tooth contact. Spatial probability distribution mapping identified a threshold for rotation speeds for radial atomization between 80 and 100,000rpm. In this operatory mode, cutting efficiency is reduced but sufficient coolant effectiveness appears to be maintained.

Conclusion: Multiple mechanisms for atomization of fluids from rotatory instrumentation exist but parameters can be controlled to modify key spray characteristics during the current crisis.

Introduction

A key challenge for the return of global healthcare systems to 'business as usual' is the inherent risk of SARS-CoV-2 transmission via emitted sprays (including aerosols and splatter) associated with commonly performed medical and dental procedures. Whilst barrier protection can shield healthcare providers, the contamination of clinical environments by sprays has led to a need to institute periods of 'fallow time', between appointments, to protect patients and staff. Fallow times are dictated by the estimated persistence of an aerosol which is an inherently multifactorial phenomenon and restricts the use and access of a defined space. Variables include room volume, air exchange rates, air flow vectors, temperature, humidity and the complex characteristics of the generated aerosol itself. In dentistry, the lack of robust evidence regarding the nature of procedurally generated sprays, contaminated with respiratory or oral fluids, has led to the instigation of extended fallow times, which can challenge the economic viability of current care provision models, restrict patient access to care and the nature of care that can be provided.

At the onset of the COVID-19 crisis, global dental care was effectively reduced to basic management of acute needs, with a focus on exodontia when advice, analgesics and antibiotics (3A's) were insufficient to address pain (CDO-Wales 2020; Hurley et al. 2020; NHS-Scotland 2020). With a deepening understanding of the new virus, the evidence-base supporting isolation, distancing, and personal protective equipment policies has been iteratively developed for societal living and healthcare. Whilst much has been gleaned from the medical setting and from population level transmission modelling, the evidence to support policies specific to the transmission risk associated with operatory dental practice is insufficient (Innes et al. 2020). Contrarily the study of dental sprays itself is not new, and rudimentary methods to measure the spread of biological materials (blood products and culturable bacteria) during dental procedures have been reported for over thirty years. These investigations identified that many routine dental procedures including cutting of tooth structure and dental cleaning can spread material that is potentially infectious throughout the operatory environment (Micik et al. 1969). Since the emergence of SARS-CoV-2, new studies have replicated these findings testing contemporary instrumentation and procedures (Allison et al. 2020). However, there has been a dependency on methods that sample dental sprays with point-based measurements using capture plates/surfaces or directional particle size counters which have inherent limitations in generalisability across settings. Key information relevant to potential SARS-CoV-2 transmission is inadequately reported including data on ranges of droplet size, emission

trajectories and droplet lifetimes. Importantly identification of which procedures are intrinsically 'atomizing' producing the smallest droplets with highest latency and those which produce high velocity larger droplets that may result in formites at distance surfaces, is poorly understood at the mechanistic level (Bourouiba 2020).

SARS-CoV-2 transmission in the community occurs primarily through expiratory emission of mucosalivary droplets during coughing, sneezing or forced vocalisation, such as shouting or singing (Ather et al. 2020) and can be spread by asymptomatic individuals. The virus is concentrated in saliva with infected patients having between 9.9 x 10^2 and 1.2 x 10^8 viral copies/mL (To et al. 2020) and is again detectable in asymptomatic individuals (Wyllie et al. 2020). In dentistry, the use of high velocity air and water streams is essential to cool rotary instrumentation used to cut enamel and dentin or high frequency instrumentation used for dental cleaning. These products can combine with saliva and inevitably cause emission in the form of structured sprays with a high level of procedure-associated variability (Abramovitz et al. 2020; Adhikari et al. 2017; Dutil et al. 2008). Although the mucosalivary fluids are diluted considerably by the introduced coolants, in contrast to a respiratory emission the operatory spray is produced over extended time periods thus generating a potentially significant exposure.

A seminal publication at the outset of COVID-19 from Lydia Bourouiba (2020) highlighted the complexity of multiphase flows in the context of respiratory emissions. The conventional wisdom that risk assessment should be based on discrimination of large and small droplets was challenged and it was concluded that understanding of the turbulent gas cloud dynamics must influence mitigation steps. Here we report, using high-speed imaging and quantitative flow analyses, the characteristics of dental sprays produced using high-speed rotary instrumentation and identify the mechanisms leading to atomisation and ejection of high velocity droplets. We highlight that by understanding these fundamental mechanisms, generalizable conclusions that are independent of the operatory setting may be made to inform spray mitigation. We propose that modification of operating parameters for rotary instrumentation (speed and coolant) can favour the formation of low velocity large droplets that have low probabilities of extending beyond the immediate proximity of the patient. This in conjunction with the prevention of mixing of the introduced spray with mucosalivary fluids using physical barriers (rubber dams) (Samaranayake et al., 1989) and capture of the spray locally with high volume aspiration may represent a demonstrable reduction in transmission risk.

Methods

Sprays generated from conventional air turbines (W&H, Austria; with water coolant and 'chip air', ~450,000 rpm) and electric micromotor (NSK, Japan; with water coolant with and without 'chip air') with 5:1 speed increasing hand-sets (X95L, NSK, Japan) were parametrically studied (from 20,000 to 200,000 rpm at 20,000rpm intervals). Measurements were undertaken in an unobstructed steady state mode, with burr contact to dental enamel (1.5 ±0.5 N) and in intra-oral simulations using a modified dental training mannequin (buccal spaces blocked out with absorbent wadding and floor of mouth with a polyvinylsiloxane 'tongue' to result in a cavity volume of ~100mL) with all surfaces pre-wetted with water before measurements to simulate oral fluids. The measurements took place within a max distance of ~0.2m from the generating spray source. This ensured a satisfactory signal to noise ratio in the imaging process and increased the overall capturing capacity of the emitted spray that would have been otherwise reduced due to the limitations imposed by its high directionality and airflow conditions, especially at a distance from the source.

A coherent and directional continuous wave 450 nm laser beam, a multidirectional 450 nm LED light source and broadband wavelength light were used to illuminate the sprays. For the laser measurement cases, the illumination was achieved through laser sheet forming optics that provided a "2 dimensional" illumination plane along the axial propagation axis of the sprays. The sprays were captured with the use of a high-speed camera (Photron FASTCAM Mini AX200 type 900K M 32GB) at variable angles, distances and frame rates. All broadband light and LED illuminated sprays were recorded with frame rates ranging between 1 and 2 kHz through "Photron's Fastcam Viewer (PFV)" software. PFV was also used to control the camera for these measurements. All laser illuminated sprays were recorded with a frame rate of 0.5 kHz through LaVision's "DaVis" software. DaVis and a LaVision PTU-X external unit was used to trigger and control the camera. The minimum spatial resolution achieved with the current setup is 100µm. It must be noted that even though the spatial resolution of our instruments could not detect individual droplets less than about 100µm, collectively these clouds of smaller droplets appear in the recording as mist which can be quantified.

Preliminary estimates of the presented droplet velocities were calculated via PFV from the broadband and LED illumination cases. The probability density maps for all laser illuminated sprays cases have been processed using DaVis. Firstly, 2000 raw images for each test case were de-warped via the use of a calibration plate. The images were subsequently binarised based on a trial and error intensity thresholding process. The intensities from all spray locations (pixels)

for every image recorded in a given case study were counted and divided by the number of images used for every test case. This allowed the generation of spatial probabilistic distributions of the spray for every test case measured. MATLAB (R2020a) was subsequently used to quantify the probability distributions of the spray for each half of the view field upstream and downstream of the spray release locations. The laser sheet illuminated sprays and associated calculations, systematically underestimate the spatial quantification of the spray due to the presence of a shadow cone cast by the burr tip, fluid film and droplets (blanked white space underneath burr at the bottom right corner of the imaging plane). Nevertheless, a systematic and parametric comparison between the cases is possible.

An optical particle size counter (Model 330, TSI Incorporated, MN, USA) with a range from 0.3 - 10μm and size resolution of < 5% at 0.5μm, was used to supplement optical measurements. The instrument was placed 1.5m from the emission source. Following baseline measurements, handpieces were fixed with burr to tooth contact and run continuously for 1min. After a further 30s to allow dispersal, data was collected (taking a further 1min). In all cases baseline conditions were re-established before further measurements were performed with typically 3 independent repeats per condition. The impact of varying the coolant parameters on heating during instrumentation was considered and methods and results are presented in Supplementary Material.

Results

Dental rotary instruments facilitate the use of high-speed rotating burrs that can apply concentrated frictional forces to remove tooth structure quickly. The devices have been traditionally powered by low torque micro air turbines (Pelton wheels) and more recently by electric micro-motors with the former requiring high rotational speeds of ~0.5 million rpm to counteract their lack of torque. Water is used to remove ablated debris, cool internal moving parts and prevent over-heating of the dental pulp. In general, for both devices air is pre-mixed (so called ‘chip air’) with water in the instrument head to ‘pre-mist’ the coolant creating a high velocity flow that exits the handset from multiple holes in its base. It is then directed to the burr tip and into the mouth in the form of a dense and fine spray. The high speed, fine mist spray is subsequently modified by its interaction with the rapidly rotating burr tip. When this spray is unobstructed (Figure 1A) it is seen to project at speeds that can exceed 12 m/s. Millions of small droplets are generated which, because of their small mass have limited gravitational effect on their trajectories. For comparison, peak exhalation velocities from sneezing have been

quantified in a range 10-30 m/s. In Figure 1A, the spray from the air turbine can be seen to increase in cross-sectional area as it disperses through the air at a shallow angle from the generation origin. A fast-moving fine mist spray core is formed, surrounded by a shear layer region, where the spray interacts with the surrounding air. The high-speed spray causes entrainment of the surrounding air and a recirculation vortex extending at the base of the handset (top and bottom from the origin of the spray). This region is formed in its majority by a fine mist and is indicated by the blue region of Figure 1B. Larger droplets, with high velocities, are randomly ejected due to the physics of the atomisation process (appearing as red streaks in Figure 1B). These droplets move along straight trajectories due to their inertia being unaffected by the air flow and therefore are not contained in the main body or recirculation regions of the spray. Such droplets are unlikely to be consistently detected using point-measurement approaches due to the stochastic nature of their formation but carry a significant mass of the introduced water flowrate.

A key problem in modelling dental procedurally generated sprays is the enormous heterogeneity in outcome due to the positioning of the generation source by the clinician as they operate on different aspects of teeth across the oral cavity, together with the interaction of the introduced flow with the mouth, its structures and its pooled mucosalivary fluids. Figure 1C emphasises this showing that the spray morphology is immediately perturbed when directed into the oral cavity (albeit here in a controlled training mannequin with simulated oral fluids and aspiration). In general, obstruction of the direct flow reduces droplet velocities and extent of spread, but a significant and notable fine mist of droplets persists with velocity, density and direction all dependent on the positioning of the tool.

Figure 2 illustrates the quantitative method used to study spray generation in this study showing a single image frame in 2A, the probability density map from >2000 images in 2B and its associated standard deviation in 2C for an unobstructed spray generated by an air turbine. A dense spray occupying the majority of the image field is produced with droplet velocities ranging from 7- 12 m/s. Data are lost from a region under the burr tip due to a shadowing of the illuminating light sheet and this represents an underestimation in the near field characterisation of the spray. This is consistent throughout all measurements reported here.

When air and water are ‘pre-misted’ prior to delivery of the coolant to the burr tip (for both air-turbines and electric motors handsets using ‘chip air’) atomization occurs due to the shear introduced by the high pressure air splitting droplets apart. To consider whether forces introduced by the rapidly rotating burr tip can also atomize, the ‘chip air’ was blocked for the

electric motor with speed increasing handset, and the spray studied as a function of decreasing revolution speed. In Figure 3 it can be seen that the spread of the spray significantly reduces with decreasing rpm, but in the plots of the standard deviation of the probability density function it can be seen that a combination of both atomized spray (fine droplet) and higher velocity droplets are both produced at a speed above 100,000 rpm. This confirms that the fluid interaction with the rotating burr tip can result in radial atomization, but a threshold (for the system studied) does exist between ~80,000-100,000 rpm where a reduction in droplet velocity and increase in droplet size (reflected as an increase in droplet trajectory curvature) was observed. Spray distribution and trajectories are further modified by tooth contact and in Figure 3 it can be seen that atomization occured at the tooth surface at revolutions >80,000 rpm, likely due to the impact of liquid fragments on variable thickness liquid films formed at the tooth surface, which has significant implications for atomization of thin salivary films also present on tooth surfaces. Trends observed in Figure 3 are quantified in Figure 4A,B and can be directly visualized in single frame images in 4C,D,E which shows the generated spray at 60,000 rpm comprised of only larger slow moving droplets all appearing to follow parabolic trajectories (under gravitational influence) within the imaging field. In Figure 5 it is seen that when the mechanisms understood to result in atomization are mitigated, achieved here by running an electric micromotor with 5:1 speed increasing handpiece with 'chip air' blocked and revolutions restricted to 60,000 rpm, in all clinically simulated positions the spray generated is minimal with no evidence of misting. Optical particle size measurements summarised in Figure 4F,G and in Supplemental Table 1 show good agreement with optical data, with droplet particle sizes <5µm only detectable above baseline levels at revolutions >80,000 rpm. Introduction of pre-misting of the coolant for the air-trubine led to a dramatic increase in all detectable particle sizes.

Discussion

The complexity and in particular the heterogeneity of generated dental sprays (including aerosols and splatter) underpins the great challenges faced by the dental profession and the risk to individuals, whilst community levels of risk for SARS-CoV-2 transmission remain at a tangible level. The so-called "universal" precautions used in dental operatory settings to protect patients and care providers were introduced primarily in response to the emergence of blood borne viruses including HIV. Unfortunately, as with so many areas of healthcare, dentistry has not prepared for the possibility of a viral respiratory pathogen that has potentially high transmittance within a dental care setting. Academic systematic review has highlighted the

paucity of high-quality evidence (Innes et al., 2020). Accordingly, there is a paucity of robust evidence to support policy makers. Notably a recent Cochrane review, published to address concerns related to risk of SARS-CoV-2 transmission in dental settings, have failed to identify adequate scientific evidence leaving dental regulators to base policies on 'expert' opinion, with interpretation of the same evidence by different bodies often being contradictory (Verbeek et al. 2020).

A significant point of contention has been how to define dental sprays and extrapolate risk based on the emerging understanding of SARS-CoV-2 transmission. Historically in dentistry, aerosols have referred to droplets less than 50 µm in diameter of which those <10 µm were considered an inhalation risk (Micik et al. 1969). This is a disparity with accepted respiratory infection classifications and for SARS-CoV-2 transmission, virally loaded airborne droplets <5 µm that remain suspended in the air for prolonged periods are considered of particular risk (Cook 2020; Kirk-Bayley et al. 2020) alongside 'splatter' of infected larger droplets that have the potential to contaminate fixed and mobile surfaces and are subsequently introduced into respiratory or ocular systems due to inadequate hand hygiene (Szymanska 2007). In this study, we demonstrate the underpinning mechanisms that lead to the formation of these features of dental sprays formed by rotary instrumentation.

We have identified four contributing mechanisms to the atomisation of coolant water or/and a mixture of coolant water and oral fluids by rotary handsets in the form of multiscale droplet sizes (including mist) and velocities. These are:

1. Pre-misted and premixed cooling water and air generated internally by air turbines and micromotors operated with chip air. A high velocity mixture of air and droplets is ejected through ports at the base of handset heads and directed to the burr tip of the instruments for cooling purposes during tooth ablating/polishing.
2. For the unobstructed cases (i.e. when the burr tip is not interacting with a tooth surface), interaction of the high angular velocity burr tips with the
    a. sprayed coolant water film established on the burr for cooling purposes
    b. other droplets
    c. pooled oral liquids

    lead to droplet formation and ejection of high speed "projectile" droplets radially or at a forward angle to the burr rotational axis and coolant ejection direction.
3. Interaction of the high angular velocity burr tips with the

a. sprayed coolant water film established on the burr for cooling purposes
b. other droplets
c. pooled oral liquids

and the tooth surface leading to an increased induced liquid shear layer between the rotating burr tip and the tooth, causing fine misting of liquids within the layer and high speed "projectile" droplets. The droplets and mist is ejected stochastically according to the orientation of the interacting surfaces.

4. Secondary processes that might cause liquid atomisation because of high speed primary atomised droplet or/and air/droplet mixture collision/interaction with other droplets, liquid films or pooled liquids within the mouth cavity that are expected to generate low speed, large size droplets.

The generalisation of findings of dental spray generation studies into the wide variety of clinical settings that exist is complex, particularly when the spray itself can be so variable. The speed, direction, size and number of droplets emerging from the oral cavity for each handset is different and is expected to change according to the type, location, orientation and specific operation of the dental instrument with respect to the interaction of the instrument and generated spray with hard and soft tissues of the oral cavity. Mixing of the introduced coolant with real saliva also requires consideration. Saliva is rheologically complex differing according to stimulation method, physiological conditions, time and between individuals. It is described as a non-Newtonian, shear thinning liquid with viscoelastic/pseudo-viscoelastic properties (Lysik et al., 2019) exhibiting Newtonian behaviour at high shear rates (Foglio-Bonda et al., 2014). Its dynamic viscosity ranges between 1-20mPas. It is expected that large dilution of saliva with excess cooling water (dynamic viscosity of 1mPas) results in a mixture expected to be rheologically more like water and was therefore not simulated in this initial study.

Here an overarching approach to assist risk assessment with dental spray generating procedures is reported. We observe that rotary instrumentation with high torque electric micromotors and 5:1 speed increasing handsets can be used without atomization or the ejection of high velocity droplets when specific operating parameters are selected. Although cutting efficiency is significantly reduced, the machining of enamel, dentine and some restorative materials is achievable with adequate cooling to prevent pulp injury still provided in the absence of 'chip air' (Supplemental Table 2, Supplemental Figures 1&2) when operated at reduced speeds (80,000-100,000rpm). The impact of these machining protocols on thermal damage at the site of the cut substrate requires further investigation but is beyond the scope of the current study.

These measures in the short term may allow many routine operatory procedures to be performed and are feasible without major infrastructural modification to surgery environments. Inevitably, risk assessments at local levels, put in context of population infection rates, mitigation factors (on which there is emerging evidence) such as barrier dams, to prevent oral fluid mixing; aspiration; air filtration and ventilation schemes; all must guide decision making, however in certain settings, such as open plan clinics that are commonly found in dental education settings, modification of instrumentation protocols is likely to be essential in the short-term.

Acknowledgments

Spray visualisation was generously supported as part of the Covid-19 response by Photron (Europe) Ltd and LaVision UK Ltd. Measurements were supported by Guy's and St Thomas NHS Foundation Trust, the British Endodontic Society and the UK Engineering and Physical Sciences Research Council: EP/V038141/1

Conflict of Interest

There are no conflicts of interest to declare

Contributions of Authors

AS, **OA** and **HY** contributed to conception and design; acquisition, analysis and interpretation; and drafted the manuscript. **WW**, **JG**, **AM**, **SP**, **CD**, **NN**, **EW** and **JJ**, contributed to conception; interpretation and critically revised manuscript. All authors gave their final approval and agree to be accountable for all aspects of the work

Figure Legends

Figure 1. (A) is a still frame from high speed imaging of an unobstructed spray from an air turbine possessing a high velocity spray, a turbulent shear layer at the periphery of the core and recirculation regions close to the burr tip. (**B)** is the same image false coloured with the central spray core in orange, a shear layer region located outside of the central core region in yellow and recirculation regions in blue. A group of high droplet velocity straight trajectories is shown by the red streaks towards the top of the image. **(C)** When the same instrument is placed inside a simulated oral cavity (palatal to the maxillary central incisors) a turbulent fine mist of a reduced but significant velocity is produced (principle direction indicated by the yellow arrow).

Figure 2 shows an instantaneous image of the spray formed by an air turbine unobstructed running in a steady state **(A)**, the probability distribution of the spray droplet concentration based on >2000 images **(B)** and its standard deviation **(C)**. For interpretation in **(B)** pixels that are red indicated a 100% chance of encountering a droplet at any point in time, pixels that are black 0%. In **(C)** standard deviation is plotted on an equivalent scale.

Figure 3. Probability density function maps of droplet concentration for a micromotor with a 5:1 speed increasing handpiece run with no 'chip air' rotating between 200,000 and 20,000 rpm. Probability density function maps are based on >2000 images for each modality with the instrument running unobstructed in steady state. At 200,000 rpm, most of the droplet velocity is ~1.4m/s which is an order of magnitude less than an air turbine. PDFs of droplet concentration (top line) and standard deviation of the concentration fluctuations (middle line) for a micromotor run with no 'chip air' rotating at decreasing speed with the burr tip in contact with wet enamel. Distributions are again based on >2000 images for each modality. Spray distribution and trajectories are modified by tooth contact. There is evidence at higher speeds that atomization near the tooth surface occurs; however with decreasing speed the coolant largely streams over the tooth surface with a limited number of low velocity droplets being deposited within the imaging field of view. Scale bars are equivalent to 50 mm in all images.

Figure 4. (A) Proportion of image field where the probability density function of droplet concentration is greater than 1% plotted against micromotor speed, for the entire imaging field in (B) (black coloured bars) and the left side of the imaging field (grey coloured bars), which is ~90 mm from the burr tip. For comparison, equivalent values for an air turbine are plotted as diamonds at the right of the histogram. We observe that reduction of micromotor speed to 60,000 rpm results in: at a distance of >90 mm away from the burr only 0.1% of the imaged pixels have >1% chance of encountering a droplet. This represents a ~280-fold reduction compared with an air turbine. (C-E) show representative sprays with an elimination of radial atomization below 100,00 rpm. F and G are histograms showing droplet particles sizes associated with non- pre-misted micromotor speed (rpm) compared with ambient baseline (BL) and air turbine with pre-misted coolant.

Figure 5. Representative images showing spray formation when mechanisms identified to cause atomization are mitigated, achieved here by running an electric micromotor with 5:1 speed increasing handpiece with 'chip air' blocked and revolutions restricted to 60,000 rpm. The burr was held in contact with the palatal surface of right maxillary central incisor (A), lingual surface of right mandibular central incisor (B), and the occlusal surface of the right mandibular first molar (C).

References

Abramovitz I, Palmon A, Levy D, Karabucak B, Kot-Limon N, Shay B, Kolokythas A, Almoznino G. 2020. Dental care during the coronavirus disease 2019 (covid-19) outbreak: Operatory considerations and clinical aspects. Quintessence Int. 51(5): 418-429.

Adhikari A, Kurella S, Banerjee P, Mitra A. 2017. Aerosolized bacteria and microbial activity in dental clinics during cleaning procedures. J Aerosol Sci. 114:209-218.

Allison JR, Currie CC, Edwards DC, Bowes C, Coulter J, Pickering K, Kozhevnikova E, Durham J, Nile CJ, Jakubovics N, et al. 2020. Evaluating aerosol and splatter following dental procedures: addressing new challenges for oral healthcare and rehabilitation. J Oral Rehabil. 2020 Sep 23;10.1111/joor.13098. doi: 10.1111/joor.13098. Online ahead of print.

Ather A, Patel B, Ruparel NB, Diogenes A, Hargreaves KM. 2020. Coronavirus disease 19 (covid-19): Implications for clinical dental care. J Endod. 46(5): 584-595.

Bourouiba L. 2020. Turbulent gas clouds and respiratory pathogen emissions: Potential implications for reducing transmission of covid-19. JAMA. 323(18):1837-1838.

CDO-Wales. 2020. Red alert phase escalation. All Wales Clinical Dental Leads COVID-19 Group. [accessed November 19 2020: https://gov.wales/sites/default/files/publications/2020-04/red-alert-phase-escalation.pdf]

Cook T. 2020. Personal protective equipment during the coronavirus disease (COVID) 2019 pandemic–a narrative review. Anaesthesia. 75(8): 920-927.

Dutil S, Mériaux A, de Latrémoille M-C, Lazure L, Barbeau J, Duchaine C. 2008. Measurement of airborne bacteria and endotoxin generated during dental cleaning. J Occup Environ Hyg. 6(2):121-130.

Foglio-Bonda A, Pattarino F, Foglio-Bonda PL, 2014. Kinematic viscosity of unstimulated whole saliva in healthy young adults. Eur Rev Med Pharmacol Sci. 18(20):2988-94.

Hurley S, Rooney E, Reece C. 2020. Preparedness letter for primary dental care - nhs. [accessed November 19, 2020]: https://www.mddus.com/coronavirus/coronavirus-update/2020/march/preparedness-letter-for-primary-dental-care

Innes N, Johnson I, Al-Yaseen W, Jones R, KC S, Mcgregor S, Robertson M, Wade W, Gallagher J, Harris R. 2020. A systematic review of aerosol and droplet generation in dentistry.

medRxiv. https://www.medrxiv.org/content/10.1101/2020.08.28.20183475v1 [accessed on November 19, 2020] preprint not peer-reviewed.

Kirk-Bayley J, Challacombe S, Sunkaraneni S, Combes J. 2020. The use of povidone iodine nasal spray and mouthwash during the current covid-19 pandemic may protect healthcare workers and reduce cross infection. SSRN; Internet, available at: https://papers.ssrn.com/sol3/papers.cfm?abstract_id=3563092

Łysik, D, Niemirowicz-Laskowska, K, Bucki, R, Tokajuk, G, Mystkowska, J. 2019. Artificial saliva: Challenges and future perspectives for the treatment of xerostomia. Int J Mol Sci. 20(13): 3199.

Micik RE, Miller RL, Mazzarella MA, Ryge G. 1969. Studies on dental aerobiology: I. Bacterial aerosols generated during dental procedures. J Dent Res. 48(1): 49-56.

NHS-Scotland. 2020. Management of acute dental problems during covid-19 pandemic. SDCEP. [accessed November 19, 2020: https://www.sdcep.org.uk/wp-content/uploads/2020/03/SDCEP-MADP-COVID-19-guide-300320.pdf]

Samaranayake LV, Reid J, Evans D. 1989. The efficacy of rubber dam isolation in reducing atmospheric bacterial contamination. ASDC J Dent Child. 56(6): 442-444

Szymanska J. 2007. Dental bioaerosol as an occupational hazard in a dentist's workplace. Ann Agric Environ Med. 14(2): 203-207.

To KK-W, Tsang OT-Y, Yip CC-Y, Chan K-H, Wu T-C, Chan JM-C, Leung W-S, Chik TS-H, Choi CY-C, Kandamby DH. 2020. Consistent detection of 2019 novel coronavirus in saliva. Clin Infect Dis. 71(15): 841-834.

Verbeek JH, Rajamaki B, Ijaz S, Sauni R, Toomey E, Blackwood B, Tikka C, Ruotsalainen JH, Balci FSK.2020. Personal protective equipment for preventing highly infectious diseases due to exposure to contaminated body fluids in healthcare staff. Cochrane Database Syst Rev 4:CD011621.

Wyllie AL, Fournier J, Casanovas-Massana A, Campbell M, Tokuyama M, Vijayakumar P, Warren, JL, Geng B, Muenker MC, Moore AJ, et al. 2020. Saliva or Nasopharyngeal Swab Specimens for Detection of SARS-CoV-2. N Engl J Med. 383(13):1283-1286.

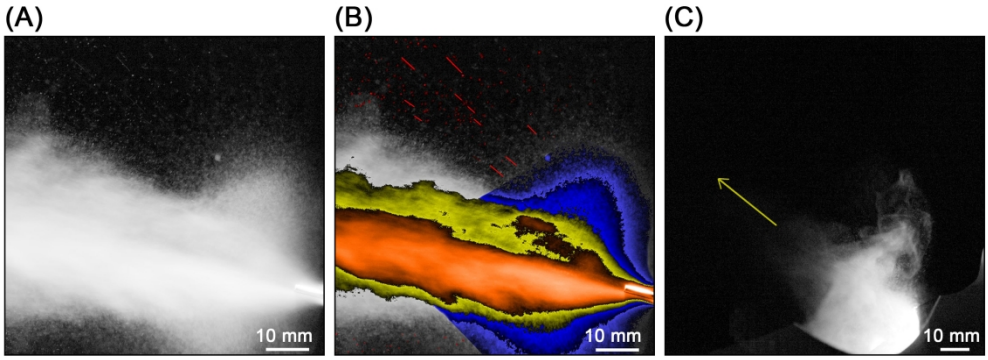

Figure 1. (A) is a still frame from high speed imaging of an unobstructed spray from an air turbine possessing a high velocity spray, a turbulent shear layer at the periphery of the core and recirculation regions close to the burr tip. (B) is the same image false coloured with the central spray core in orange, a shear layer region located outside of the central core region in yellow and recirculation regions in blue. A group of high droplet velocity straight trajectories is shown by the red streaks towards the top of the image. (C) When the same instrument is placed inside a simulated oral cavity (palatal to the maxillary central incisors) a turbulent fine mist of a reduced but significant velocity is produced (principle direction indicated by the yellow arrow).

155x56mm (600 x 600 DPI)

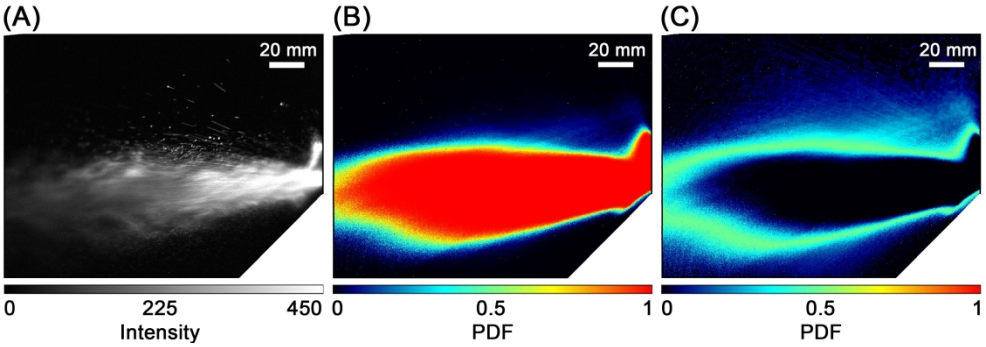

Figure 2 shows an instantaneous image of the spray formed by an air turbine unobstructed running in a steady state (A), the probability distribution of the spray droplet concentration based on >2000 images (B) and its standard deviation (C). For interpretation in (B) pixels that are red indicated a 100% chance of encountering a droplet at any point in time, pixels that are black 0%. In (C) standard deviation is plotted on an equivalent scale.

156x53mm (600 x 600 DPI)

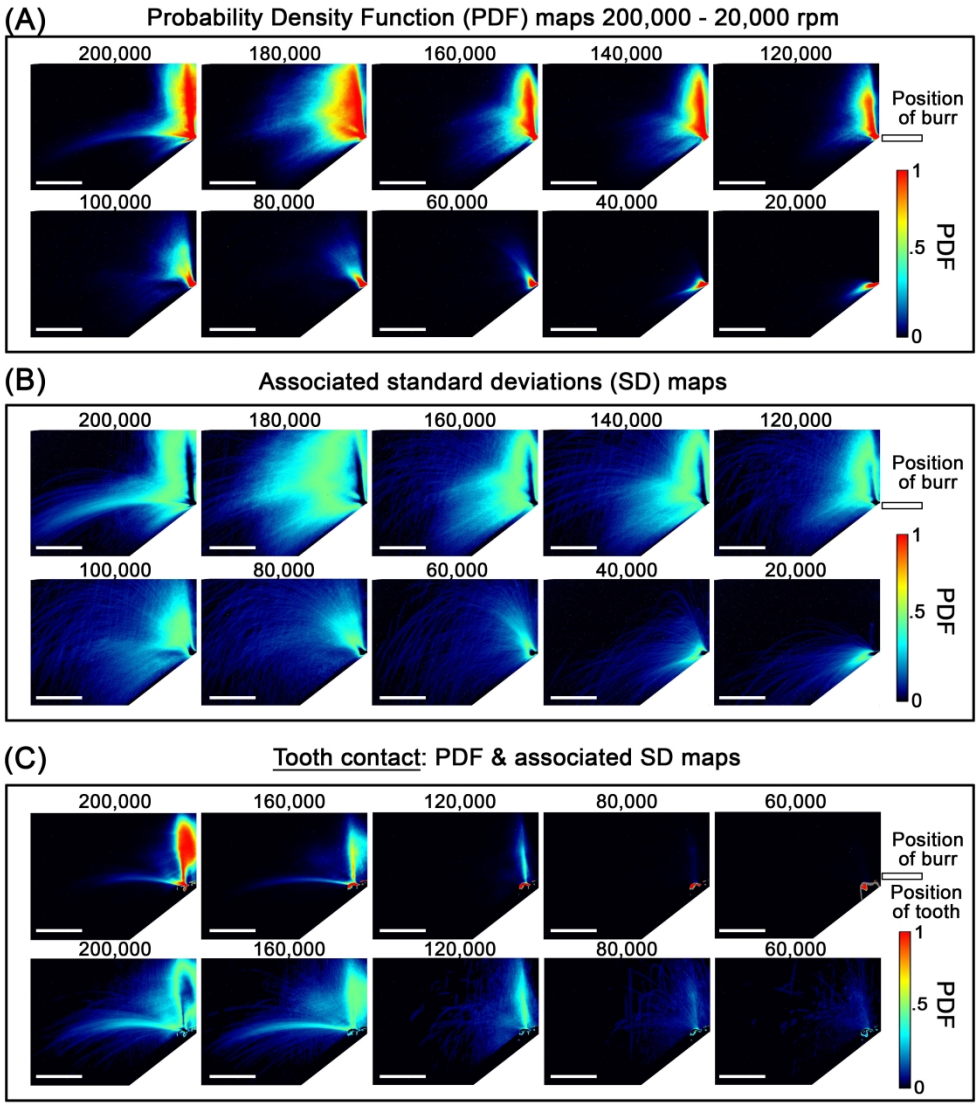

Figure 3. Probability density function maps of droplet concentration for a micromotor with a 5:1 speed increasing handpiece run with no 'chip air' rotating between 200,000 and 20,000 rpm. Probability density function maps are based on >2000 images for each modality with the instrument running unobstructed in steady state. At 200,000 rpm, most of the droplet velocity is ~1.4m/s which is an order of magnitude less than an air turbine. PDFs of droplet concentration (top line) and standard deviation of the concentration fluctuations (middle line) for a micromotor run with no 'chip air' rotating at decreasing speed with the burr tip in contact with wet enamel. Distributions are again based on >2000 images for each modality. Spray distribution and trajectories are modified by tooth contact. There is evidence at higher speeds that atomization near the tooth surface occurs; however with decreasing speed the coolant largely streams over the tooth surface with a limited number of low velocity droplets being deposited within the imaging field of view. Scale bars are equivalent to 50 mm in all images.

165x185mm (600 x 600 DPI)

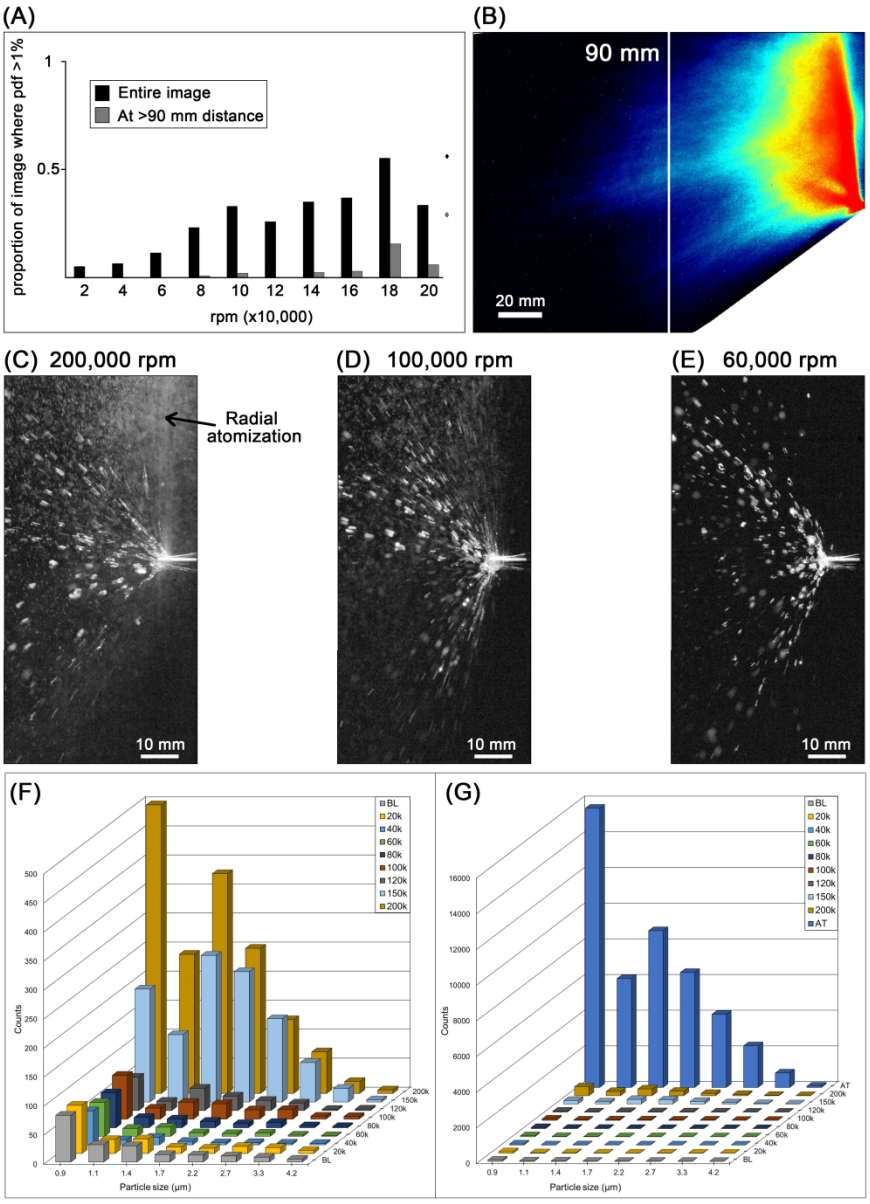

Figure 4: (A) Proportion of image field where the probability density function of droplet concentration is greater than 1% plotted against micromotor speed, for the entire imaging field in (B) (black coloured bars) and the left side of the imaging field (grey coloured bars), which is ~90 mm from the burr tip. For comparison, equivalent values for an air turbine are plotted as diamonds at the right of the histogram. We observe that reduction of micromotor speed to 60,000 rpm results in: at a distance of >90 mm away from the burr only 0.1% of the imaged pixels have >1% chance of encountering a droplet. This represents a ~280-fold reduction compared with an air turbine. (C-E) show representative sprays with an elimination of radial atomization below 100,00 rpm. (F) and (G) are histograms showing droplet particles sizes associated with non- pre-misted micromotor speed (rpm) compared with ambient baseline (BL) and air turbine with pre-misted coolant.

157x216mm (600 x 600 DPI)

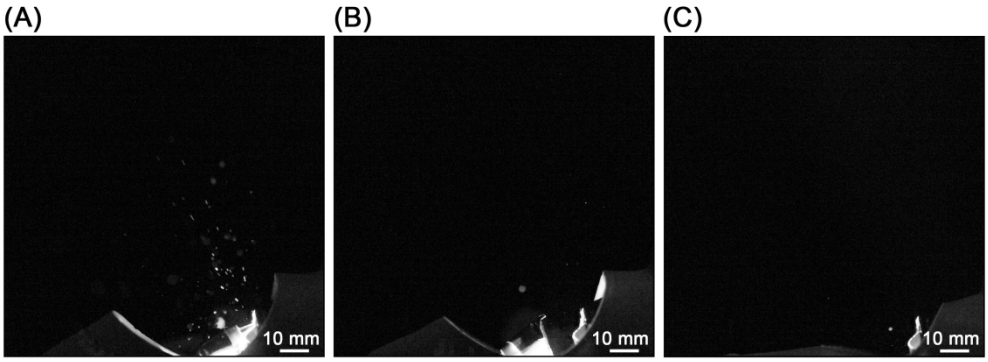

Representative images showing spray formation when mechanisms identified to cause atomization are mitigated, achieved here by running an electric micromotor with 5:1 speed increasing handpiece with 'chip air' blocked and revolutions restricted to 60,000 rpm. The burr was held in contact with the palatal surface of right maxillary central incisor (A), lingual surface of right mandibular central incisor (B), and the occlusal surface of the right mandibular first molar (C).

155x57mm (600 x 600 DPI)

"Mechanisms of atomization from rotary dental instruments and its mitigation"

Supplemental Material

Methods:

The effectiveness of cooling achieved when a micromotor with a 5:1 speed increasing handpiece was used with 'chip-air' blocked was assessed on a thermally conductive substrate (brass) and on bovine dentine. Temperature measurements were made using a standardized experimental set-up initially at room temperature. A 2 mm of brass plate was machined using a 541 pattern burr for each condition and K-type thermocouples placed in intimate contact with the contra-lateral surface with simultaneous monitoring of the incoming coolant temperature at 10 Hertz using a Pico TC-08 datalogger accurate to 0.1°C (note that with increasing motor use, the unit heats the incoming coolant slightly with time).

A further series of measurements were conducted with the substrate thermally held at initially at ~36.5°C to identify whether the incoming coolant (fed at a lower temperature of ~23°C) still acted to reduce overall temperature effectively. Measurements were performed on both brass and bovine dentine. Machining was stopped when ~1mm of material over the thermocouple had been removed.

Results:

Supplemental Table 1.

Size (µm)	BL	20,000 rpm	40,000 rpm	60,000 rpm	80,000 RPM	100,000 rpm	120,000 rpm	150,000 rpm	200,000 rpm	Air Turbine
0.3	4071 ± 204	3920	3937 – 3964	3388 – 3618	3210 – 3381	3158 - 4081	2960 - 4121	3127 - 5630	3556 – 5723	76118 –113734
0.38	1255 ± 86	1229	1195 - 1212	1135 - 1152	1077 - 1109	1055 - 1333	945 - 1329	943 - 1694	1212 - 1771	49408 – 65818
0.47	370 ± 87	494	259 – 489	396 – 455	335 -349	325 - 368	313 - 315	406 – 455	523-564	34360 – 48935
0.58	160 ± 7	186	152 – 191	144 – 157	126 -133	127 - 152	116 – 149	156 - 358	384-447	21383 - 36458
0.72	57 ± 14	51	39 – 72	49 -58	48 -63	47 – 58	57 – 62	82 – 169	275 - 306	11502 – 18693
0.90	80 ± 13	83	53 – 64	54 - 65	56 -67	72 – 79	52 – 63	122 – 267	458 - 536	15659 – 29598
1.12	30 ± 4	24	8 – 9	12 -15	13 - 20	18 – 20	16 – 27	69 – 163	204 - 275	6106 – 10570
1.39	28 ± 7	25	3- 23	14 -18	12 -17	28 – 30	27 – 50	164 – 341	306 - 451	8793 – 14317
1.73	13 ± 3	11	3 – 9	5 -7	8 -14	24 – 29	16 – 34	122 – 327	189 - 311	6452 – 11299
2.16	12 ± 3	9	2 – 5	2 - 7	5 -8	13 – 19	11 – 24	72 – 215	105 - 149	4107 – 7579
2.69	10 ± 3	12	1 - 7	4 - 6	6 -13	15 – 18	8.0 – 18	18 -118	56 - 87	2340 – 4897
3.34	8 ± 3	10	1 - 5	1 - 3	1 -5	4 – 6	1 – 3	5 -42	8 - 33	815 – 2682
4.16	5 ± 2	5	0 - 5	0 -1	0 - 2	3 – 6	2 - 3	2 -5	1 –11	81 – 925

Binned counts of droplet particle sizes recorded at a fixed distance of 1.5 meters from the emission source after 1 min of instrument operation for electric micromotors and speed increasing handpieces with no premisting running at 20,000 to 200,000 rpm and for an air turbine with premisting running at ~450,000 rpm. Mean and standard deviations are provided for baseline (BL) where n=6. A single measurement was obtained for 20,000 rpm and for all other values ranges are provided (n=3). Data is reproduced in Figure 4.

Supplemental Table 2.

Revolutions per minute (rpm)	200k	160k	120k	80k	60k	40k
Temp rise above coolant temp after 15s (°C)	1.5±1.1	0.7±0.4	0.4±0.1	0.5±0.4	0.4±0.1	0.4
Temp rise above coolant temp after 45s (°C)					0.9	

Coolant at 22.5-23.0 °C

Mean temperature rise (and associated standard deviation) above incoming coolant temperature following machining of standardised brass plates (2 mm thickness) with a 541 pattern burr, at various motor speeds (rpm) with 'chip-air' blocked preventing pre-misting of the coolant (n=3). Data demonstrates at non-atomising rotary speeds relevant to the primary objective of this report only a minor temperature rise (<1°C) was measured on the contralateral surface of the machined substrate after short and more prolonged cutting periods.

Supplemental Figure 1.

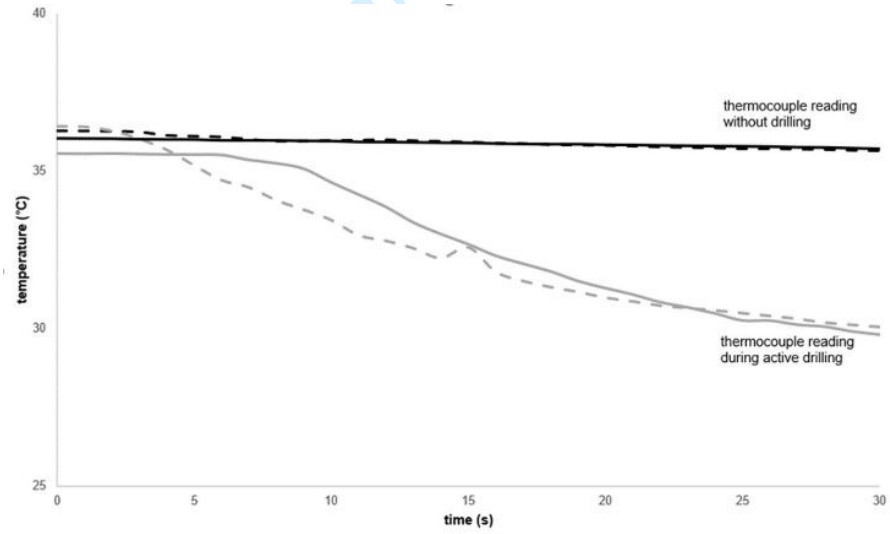

Thermal data of the test substrate held at ~35.5°C to approximate physiological temperature with and without machining at 60,000 rpm with a 541-pattern burr with 'chip-air' blocked. With no drilling the temperature control remained constant. Drilling for 30s with no pre-misting of the incoming water resulted in a cooling of the system plateauing as the temperature approached that of the coolant demonstrating continued effectiveness of the coolant in this experimental set-up.

Supplemental Figure 2.

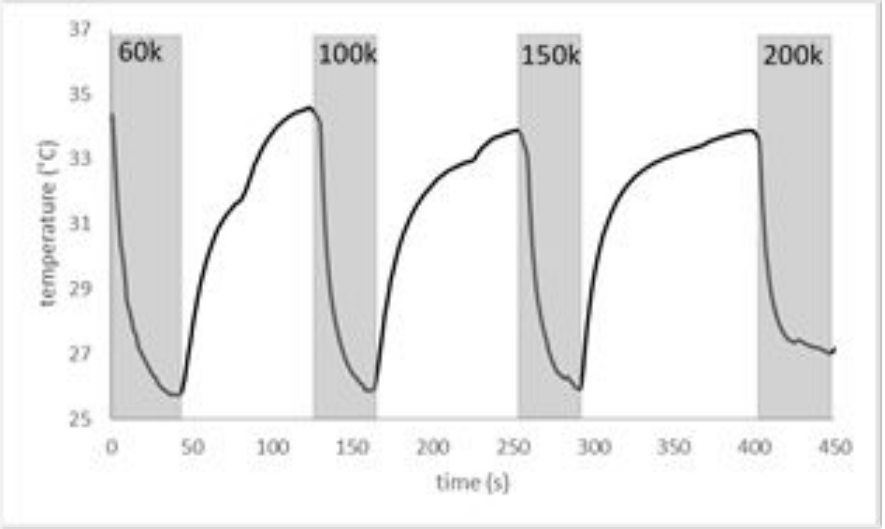

The figure shows temperature measurements made during cutting of 2 mm thickness bovine dentine plates held at a temperature of ~35°C. Regions highlighted in grey indicate active cutting of the substrate to a 1 mm minimum thickness from the thermocouple at various rpm with a 541-pattern burr with 'chip-air' blocked. Cooling effectiveness reduces with increasing rpm (60k, 100k, 150k and 200k) but a significant net reduction in the overall temperature of the substrate for each mode indicates suitable cooling is still achieved (i.e. no net increase above physiological temperature at the thermocouple position simulating the pulp).